AURORA: a Time-Dependent Multi-stream Electron Transport Code

Björn Gustavsson

November 18, 2019

Introduction

This document contains the documentation of AURORA the time-dependent multi-stream electron-transport code. This documentation lays out the mathematic-physical approach of AURORA and documents the collision-cross-sections, phase-functions and secondary-electron spectra used. For a more exhaustive presentation of AURORA and its capacities see Gustavsson (2019/2020 JGR).

Time-Dependent Multi-Stream Electron Transport Equation

The temporal and spatial variation of energetic electron fluxes in the ionosphere can be modeled with the Boltzmann equation for phase-space density, f. Since the electron transport is much smaller perpendicular to the magnetic field than parallel with it, we can simplify the problem to a one-dimensional Boltzmann equation by only accounting for field-aligned motion of electrons (Schunk & Nagy, 2009; Guio, 1998, e.g.):

$$\frac{\partial f}{\partial t}+\mu v\frac{\partial f}{\partial s}+\frac{q_e}{m}\mathbf{E}_{\parallel}\mu\frac{\partial f}{\partial v}+\left(\frac{q_e}{m}\mathbf{E}_{\parallel}-\frac{v^2}{2B}\frac{dB}{ds}\right)\frac{1-\mu^2}{v}\frac{\partial f}{\partial \mu}=\frac{\delta f}{\delta t}_{coll} \qquad (1)$$

where f is the phase-space density, t is the time, s is the distance along the magnetic field, v is the velocity, $\mu=\cos\theta$ where θ is the pitch-angle, $\mathbf{E}_{\parallel}$ is the electric-field component along the magnetic field, and B is the magnetic field-strength. After making the approximation that the field-aligned electric field component and the converging magnetic field have a negligible effect on f in the ionosphere (Peticolas & Lummerzheim, 2000) and transforming coordinates from velocity to energy and from distribution function to electron flux we arrive

at the time-dependent electron transport equation

$$\begin{aligned}\frac{1}{v(E)}\frac{\partial I(E,s,\mu,t)}{\partial t}+\mu\frac{\partial I(E,s,\mu,t)}{\partial s} =& -A\,I(E,s,\mu,t)\\ &+B(E,s,\mu,t,I)\\ &+Q(E,s,\mu,t,I)\\ &+n_e\frac{\partial(L_{ee}(E)I(E,s,\mu,t))}{\partial E}\end{aligned} \tag{2}$$

The first term on the right-hand side represents losses of electron flux from energy, E, and pitch angle-cosine, μ, due to elastic collisions changing the pitch angle and by inelastic collisions changing energy and possibly pitch-angle, with

$$A=\sum_k n_k(s)\sigma_k^{tot}(E)$$

where $\sigma_k^{tot}(E)$ is the total cross section for collisions of electrons with energy E with the k-th species. From here on, k, j, i, and ι will be used as indices; they are not used as unique identifiers. The second term on the right-hand side represents elastic scattering of electrons from other pitch angles, μ', to pitch angle μ:

$$B(E,s,\mu,t,I)=\sum_k n_k(s)\sigma_k^{el}(E)\cdot\int_{-1}^{1}p_k^{el}(E,\mu'\to\mu)I(E,s,\mu',t)d\mu'$$

where $p_k^{el}(E,\mu'\to\mu)$ is the probability that an electron at energy E with pitch angle μ' will scatter to pitch angle μ for elastic collisions with particles of species k. To calculate these probabilities we use phase-functions derived from (Porter, Varosi, & Mayr, n.d.) extended and updated with data from (Linert, King, & Zubek, 2004) for molecular oxygen and (Kanik, Johnson, Das, Khakoo, & Tayal, 2001) for atomic oxygen. The third term on the right-hand side, $Q(E,s,\mu,I)$, combines all internal sources of energetic electrons, i.e. production of photo-electrons and secondary electrons, and electrons cascading to energy E from higher energies, ε, due to inelastic collisions:

$$\begin{aligned}Q(E,s,\mu,t,I) = \;& Q_{local}(E,s,\mu,t)+\\ &\sum_k n_k(s)\sum_j\sigma_k^j(\varepsilon\to E)\int_{-1}^{1}p_k^j(\varepsilon,\mu'\to\mu)I(\varepsilon,s,\mu',t)d\mu'+\\ &\sum_k n_k(s)\int_{E+E^*}^{\infty}\sigma_k^{ion}(\varepsilon\to E)\int_{-1}^{1}p_k^{ion}(\varepsilon,\mu'\to\mu)I(\varepsilon,s,\mu',t)d\mu'd\varepsilon\end{aligned} \tag{3}$$

where the summations in the second term are over all the excited states j of the k-th species. Electrons exciting an atom or a molecule lose a quanta of energy

corresponding to the excitation energy, ΔE. Therefore electrons at energy ε that collide inelastically will contribute to the second term of Q at a series of discrete energies, $E = \varepsilon - \Delta E_k^j$ corresponding to the excitation thresholds of neutral species k. In ionizing collisions, represented with the third term in equation (3), the energy loss of primary electron is the sum of the ionization energy and the energy of the secondary electron. The fourth term on the right-hand side of Equation (2) accounts for the loss due to energy transfer to ambient electrons of density $n_e(s)$ and temperature T_e (Swartz, Nisbet, & Green, 1971). Since the flux $I(E, s, \mu, t)$ depends not only on fluxes at all higher energies but also on fluxes with all other pitch-angles equation (2) has to be solved simultaneously in a set of coupled PDEs for all pitch-angles, combined with the corresponding initial and boundary conditions. The boundary condition at the upper boundary are typically time-variations of downward fluxes at all energies and pitch-angles, either obtained from observations or simulations, or chosen (more arbitrarily) for modelling. For the upward fluxes the "most natural" boundary-condition is to set the gradients to zero — since the scattering decreases with the exponentially decreasing neutral density and the upper boundary is at an altitude where the scattering is negligibly small. The lower boundary is best handled by using an altitude low enough that the fluxes are so negligibly small that we can set the boundary condition for all pitch-angles and energies to zero.

Energetic electrons effectively only undergo energy degradation in the ionosphere – also for the time-dependent case. A consequence of this is that we can solve equation (2) from the highest energy, for which Q is zero, and then calculate all the fractions of electrons that collide inelastically and degrade to lower energies which gives us the contributions to $Q(E, s, \mu, t, I)$ for all (E, s, μ, t), and then proceed to iteratively solve equation (2) for the next lower energy.

To solve the set of equations (2) we discretize in energy, with an n_E element non-uniform energy-grid from 2 eV to the highest energy and divide the flux into n_μ discrete pitch-angle-bins, covering pitch-angles from 0 to 180 degrees, or from $\mu = -1$ to $\mu = 1$, with pitch-angle limits $\tilde{\mu}_0, \tilde{\mu}_1, \cdots, \tilde{\mu}_{n_\mu+1}$. The first step towards a discretized version of equations (2) is to rewrite the energy differential describing the electron-electron collisions. For the time-dependent electron transport this is most clearly written as

$$n_e \frac{\partial(L_{ee}(E)I(E,\mu))}{\partial E} \rightarrow \frac{1}{v(E_{i+1})}\frac{\partial \varepsilon_{ee}}{\partial t}\frac{I^{\mu_l}(E_{i+1})}{\Delta E_{i+1}} - \frac{1}{v(E_i)}\frac{\partial \varepsilon_{ee}}{\partial t}\frac{I^{\mu_l}(E_i)}{\Delta E_i} \qquad (4)$$

Here $\partial\varepsilon_{ee}/\partial t$ is the electron energy-loss-rate (Swartz et al., 1971):

$$\frac{\partial \varepsilon_{ee}}{\partial t} = \frac{3.0271 \cdot 10^{-10} n_e^{0.97}}{E^{0.44}} \left(\frac{E - E_e}{E - 0.53E_e}\right)^{2.36} \quad (eV/s)$$

where n_e and E_e are the electron density (in m^{-3}) and the thermal energy (in eV) respectively and E is the electron energy (in eV). The second term in the discretized form for electron-electron loss in equation (4) is a linear loss term for electron flux at E_i and can be merged into A in equation (2) (Gronoff, Simon Wedlund, Mertens, & Lillis, 2012, e.g.), while the first term is a source of

electrons to energy-bin E_i from the next higher energy-bin, which can be added to Q in equation (3). This turns equation (2) into an equation for the stream μ_l with pitch-angle-cosines from $\tilde{\mu}_l$ to $\tilde{\mu}_{l+1}$:

$$\begin{aligned}\frac{1}{v(E_i)}\frac{\partial I^{\mu_l}(E_i,s,t)}{\partial t}+\bar{\mu}_i\frac{\partial I^{\mu_l}(E,s,t)}{\partial s} =& -A'\,I^{\mu_l}(E_i,s,t)\\ &+\sum_{\mu_k}B'(E,s,\mu_k\rightarrow\mu_l)I^{\mu_k}(E_i,s,t)\\ &+Q'(E_i,s,\mu_l,t)\end{aligned} \tag{5}$$

where $\bar{\mu}_i$ is the average of the pitch-angle-cosine for electrons in stream i, i.e.

$$\bar{\mu}_l=\int_{\theta_l}^{\theta_{l+1}}\cos\theta\sin\theta d\theta\Big/\int_{\theta_l}^{\theta_{l+1}}\sin\theta d\theta.$$

Here we assume that the electron flux inside a pitch-angle stream is isotropically distributed between its pitch-angle limits. In this discretized version of the transport equation A' is the sum of the neutral densities multiplied with the total collision cross-section and the electron-electron loss-rate, in the second term on the right-hand side, B' is slightly modified to account for both the discretization in μ as well as correcting for the fact that a fraction of the inelastic collisions, with excitation energy ΔE_k^j, will lead to energy degradation to energies between E_i and $E_i+\Delta E_i$; and to account for scattering from all pitch-angles in streams μ_l to all pitch-angles in stream μ_l:

$$\begin{aligned}B'(E_i,s,\mu_\iota\rightarrow\mu_l)=&\sum_k n_k(s)\sigma_k^{el}(E_i)\int_{\tilde{\mu}_\iota}^{\tilde{\mu}_{\iota+1}}\int_{\tilde{\mu}_l}^{\tilde{\mu}_{l+1}}p_k^{el}(E_i,\mu'\rightarrow\mu)I(E_i,s,\mu',t)d\mu' d\mu+\\ &\sum_k n_k(s)\sum_j\sigma_k^j(E_i)\int_{\tilde{\mu}_\iota}^{\tilde{\mu}_{\iota+1}}\int_{\tilde{\mu}_l}^{\tilde{\mu}_{l+1}}p_k^j(E_i,\mu'\rightarrow\mu)I(E_i,s,\mu',t)d\mu' d\mu\cdot\\ &\max(0,1-\Delta E_k^j/\Delta E_i).\end{aligned} \tag{6}$$

Q' is modified correspondingly.

equation (5) still has to be solved simultaneously in a set with similar equations for all streams, μ_l, but with the discretization into pitch-angle-streams we can now write the full set of equations (5) for streams in all pitch-angles:

$$\frac{1}{v}\frac{\partial}{\partial t}\begin{bmatrix}I^1\\I^2\\\vdots\\I^n\end{bmatrix}+\frac{\partial}{\partial s}\begin{bmatrix}\bar{\mu}_1 I^1\\\bar{\mu}_2 I^2\\\vdots\\\bar{\mu}_n I^n\end{bmatrix}=\begin{bmatrix}-A'+B'_{11} & B'_{21} & \cdots & B'_{n1}\\ B'_{12} & -A'+B'_{22} & \cdots & B'_{n2}\\ \vdots & \vdots & \ddots & \vdots\\ B'_{1n} & B'_{2n} & \cdots & -A'+B'_{nn}\end{bmatrix}\begin{bmatrix}I^1\\I^2\\\vdots\\I^n\end{bmatrix}+\begin{bmatrix}Q^1\\Q^2\\\vdots\\Q^n\end{bmatrix} \tag{7}$$

Here I^k is an n_z-column-array with altitude-variation of electron flux in stream k at time t. The matrix on the right-hand side is $(n_z n_\mu \times n_z n_\mu)$ composed of n_μ by n_μ diagonal sub-matrices (of size $n_z \times n_z$), A' with the altitude-varying total collision cross-section, and B'_{kl} with the collisional scattering from stream k to stream l – the sum of the elastic collisions and the fraction of inelastic collision that lead to the electrons maintaining an energy between E_i and $E_i + \Delta E_i$. Integration of equation (7) is done with a standard Crank-Nicolson scheme modified to use up-stream spatial differences instead of centralized spatial differences. The boundary conditions have to be imposed for the first and last component of each of the sub-arrays I^k. To ensure stability of the solution for any type of discontinuous changes in I^k the time-step, Δt, of the Crank-Nicolson integration are chosen such that the Courant-number, $|v(E_i)\Delta t/\Delta s|$, is smaller than 1 at all energies. Further, a requirement for the discretization is that Δs should not be larger than the electron mean-free-path. This we achieve by applying an approximately 150 m step-size in altitude from 100 to 140 km transitioning to an exponentially growing step-size to the highest altitude at 649 km. The two primary consequences of these design-choices are, firstly, that for high-energy electrons the step-size in time becomes so short (≈ 3 μs, for 7 keV electrons), that is is both computationally impossible and physically irrelevant to save the solution at every time-step of the integration – instead the solution is stored with time-resolution of 1–20 ms. Secondly, that it is difficult to model precipitation with energies much larger than 10 keV since that would require a lower border at an altitude below 100 km, where the electron mean-free-path is rapidly decreasing – which would necessitate a much finer altitude-grid, leading to a significant reduction of the time-step in the Crank-Nicolson integration. With all these considerations, the number of pitch-angle streams, n_μ, that currently can be handled with a standard 2016 desktop computer in a reasonable time is approximately 10, this limits how well smooth pitch-angle distributions can be modeled at this point in time. In this work we used 10 pitch-angle-streams with pitch-angle boundaries at 0, 10, 30, 60, 80, 90, 100, 120, 150, 170 and 180 degrees from $\mathbf{B}$.

The field-aligned velocity components, $v_\parallel$, of electrons in a energy and pitch-angle cell, $[E_i, E_i + dE_i) \times [, \mu_j \mu_j + \Delta\mu_j)$, will have a spread between

$$v(E_i)\mu_{j+1} \leq v_\parallel \leq v(E_i + dE_i)\mu_j$$

where $v(E)$ is the velocity of electrons with energy E. For 1 keV electrons this leads to a 1.0 per cent spread around the average field-aligned velocity component in the $0^\circ - 10^\circ$ stream, a 6.7 percent spread in the $10^\circ - 30^\circ$ stream, which both are unproblematic. For electrons in the $30 - 60^\circ$ stream the spread grows to 27 per cent, which makes the assumption that all electrons in an energy and pitch-angle cell moves with the average field-aligned velocity problematic. To mitigate this problem a small diffusive term, with pitch-angle and energy-varying diffusivity, is added to the right-hand-side matrix in equation (7). In addition to account for the variation in field-aligned velocity, multiple pitch-angle streams are required to accurately model the length-distribution of electron-trajectories through the ionosphere, which impacts the ionization and excita-

tion profiles. This aspect of the electron transport the 10-stream calculation accounts for well. Finally, a large number of pitch-angle streams are necessary to model precipitation with general pitch-angle distributions - with 10 streams with pitch-angle boundaries at 0, 10, 30, 60, 80, 90, 100, 120, 150, 170 and 180 degrees from **B** this is impossible to do well, a far larger number of streams is required to keep the solid-angles of the streams reasonably similar. The 10-streams used is sufficient for modeling precipitation that is either isotropic or field-aligned to within 10 or 30 degrees from **B**.

Cross-sections, Phase-functions and Secondary-Electron Spectra

In order to calculate the collision effects modeled with the A and B-matrices it is necessary to have at least an estimate of the neutral density profiles. For this AURORA as default is to use the NRLMSIS-00 neutral atmosphere (Hedin, 1991; Picone, Hedin, Drob, & A.C. Aikin, 2002) for 69.58° N, 19.23° E (location of the EISCAT Tromsø site, Tromsø, Norway, where the magnetic inclination is approximately 77°) at 22 UT 20051008, as show in Figure 1.

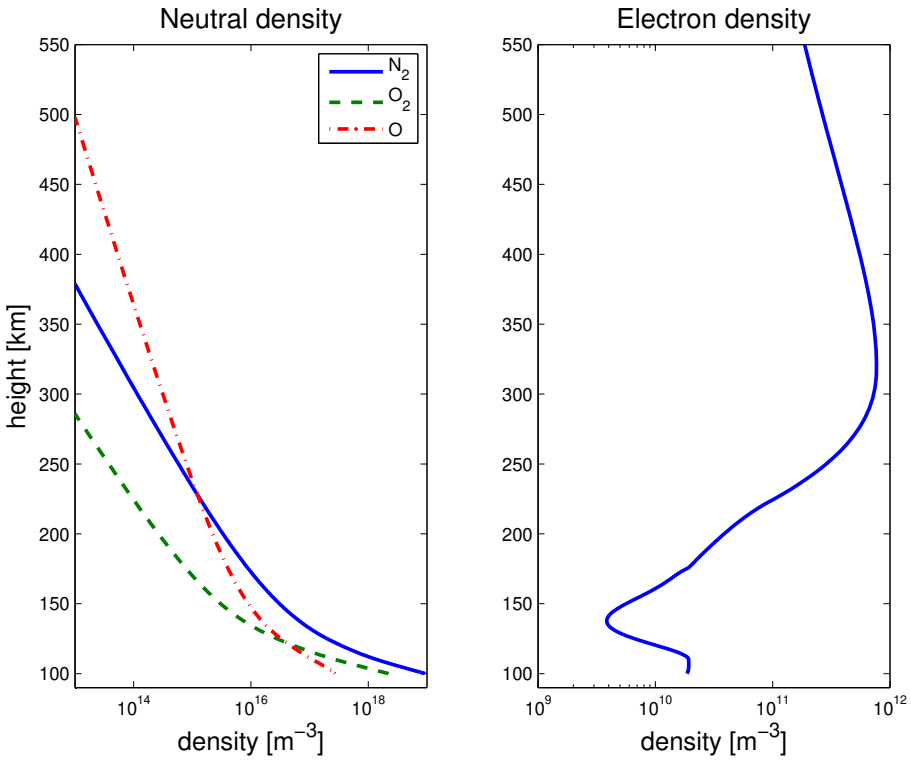

Figure 1: The density profiles for the major thermospheric constituents used are shown in the left panel. The right panel displays the electron density profile.

Further, to calculate the probability of collisions estimates of collision-cross-sections, as modeled in equations (2) to (7), AURORA uses cross-sections collected by (Itikawa et al., 1986), (Itikawa et al., 1989) and (Itikawa & Ichimura, 1990), as shown in Figures 2, 4 and 3.

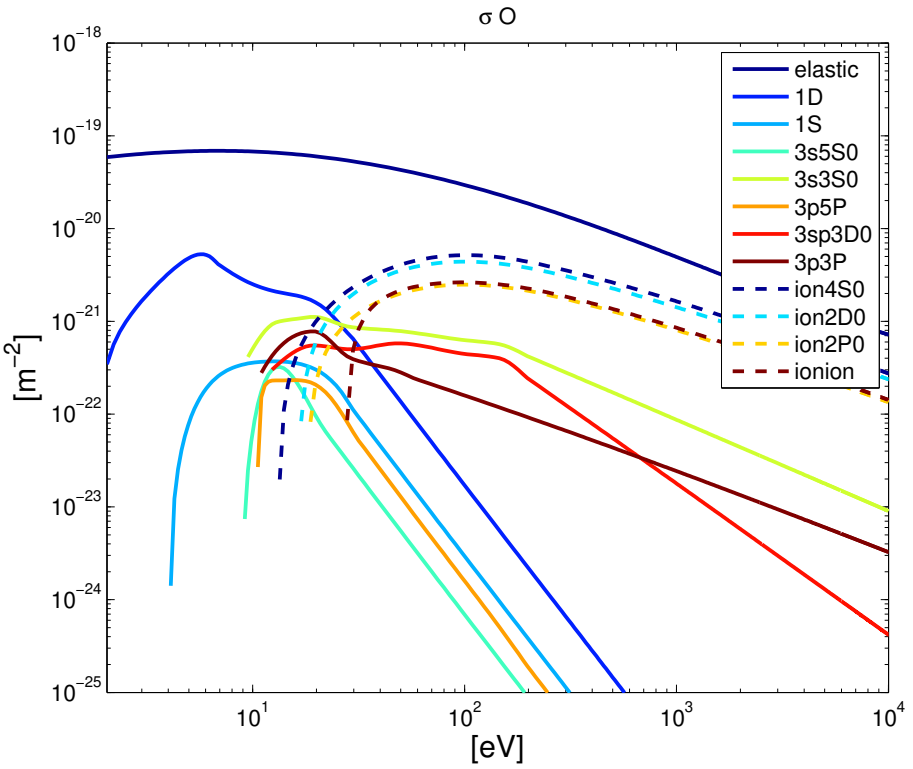

Figure 2: The cross-sections for electron-collisions with atomic oxygen are shown as functions of energy. They are: 1 elastic, 2 O(^{1}D), 3 O(^{1}S), 4 O(3s^{3}5S$_0$), 5 O(3s^{3}3S$_0$), 6 O(3p^{5}P), 7 O(3s$'^3$D$_0$), 8 O(3p^{3}P), 9 O$^+$($4S_0$), 10 O$^+$($2D_0$), 11 O$^+$($2P_0$), 12 O^{++}.

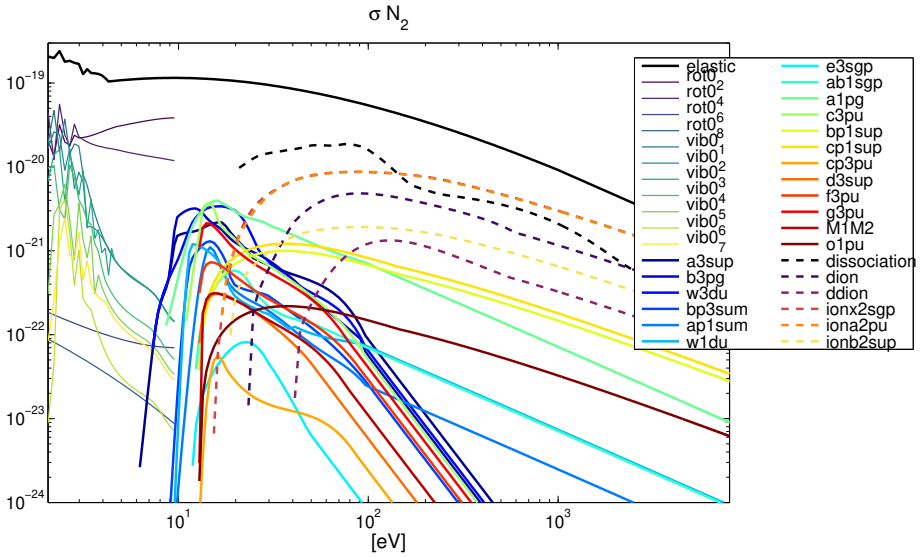

Figure 3: The cross-sections for electron-collisions with molecular nitrogen are shown as functions of energy. They are: 1 elastic, 2-5 rotational excitations 0-2, 0-4, 0-6 and 0-8, 6-12 vibrational excitations 0-1 to 0-7, 13 $N_2(A^3\Sigma_u^+)$, 14 $N_2(B^3\Pi_g)$, 15 $N_2(W^3\Delta_u)$, 16 $N_2(B'^3\Sigma_u^-)$, 17 $N_2(a'^1\Sigma_u^-)$, 18 $N_2(w^1\Delta_u)$, 19 $N_2(E^3\Sigma_g^+)$, 20 $N_2(a''^1\Sigma_g^+)$, 21 $N_2(a^1\Pi_g)$, 22 $N_2(C^3\Pi_u)$, 23 $N_2(c'^1\Sigma_u^+)$, 24 $N_2(C'^3\Pi_u)$, 25 $N_2(D^3\Sigma_u^+)$, 26 $N_2(F^3\Pi_u)$, 27 $N_2(G^3\Pi_u)$, 28 N_2(M1M2), 29 $N_2(o_4{}^1\Pi_u)$, 30 dissociation, 31 $N + N^+$, 32 $N^+ + N^+$, 33 $N_2^+(X^2\Sigma_g^+)$, 34 $N_2^+(A^2\Pi_u)$, 35 $N_2^+(B^2\Sigma_u^+)$.

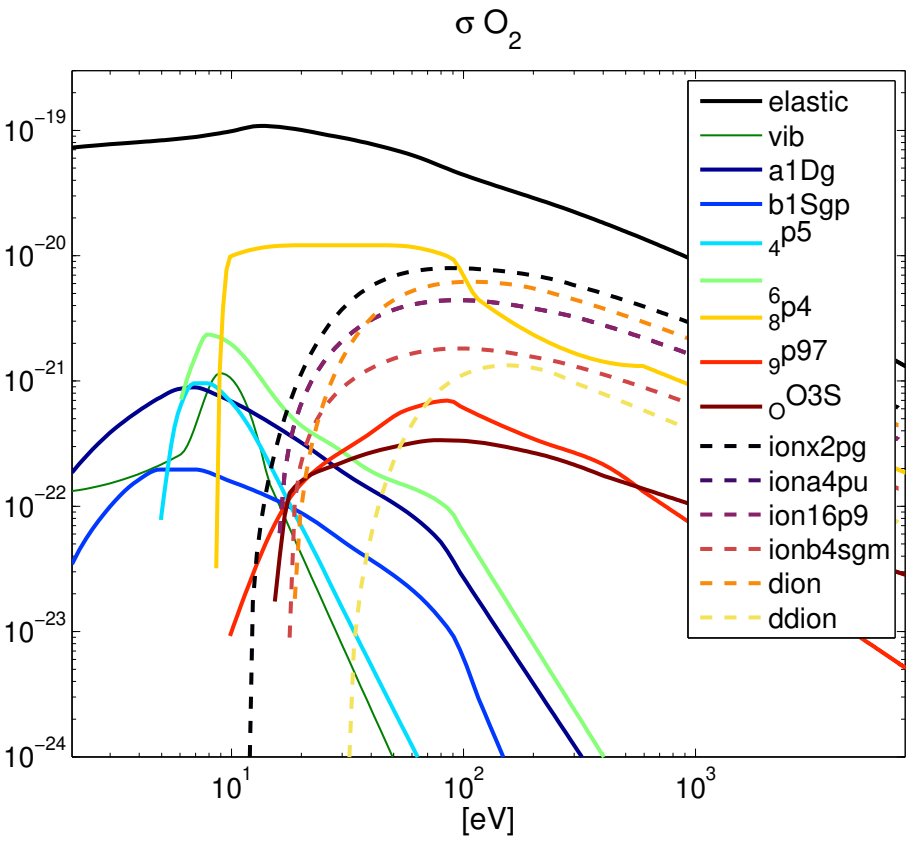

Figure 4: The cross-sections for electron-collisions with molecular oxygen are shown as functions of energy. They are: 1 elastic, 2 O_2(vib), 3 $O_2(a^1\Delta_g)$, 4 $O_2(b^1\Sigma_g^+)$, 5 4.5 eV, 6 6 eV, 7 8.4 eV, 8 9.97 eV, 9 O_2(3S), 10 $O_2(X^2\Pi_g)$, 11 $O_2^+(a^4\Pi_u)$, 12 O_2^+(16.9 eV), 13, $O_2^+(b^4\Sigma_g^-)$ 14, O^+ + O, 15, O^++O^+.

The neutral density and collision cross-section are sufficient to calculate the total number of a collision of electrons at altitude s with energy E in pitch-angle-stream μ: $I(s, E, t, \mu)n_j(s)\sigma_j^k(E)dE$, however, in collisions electrons are also changing direction by a scattering-angle, ψ, as illustrated in figure 5.

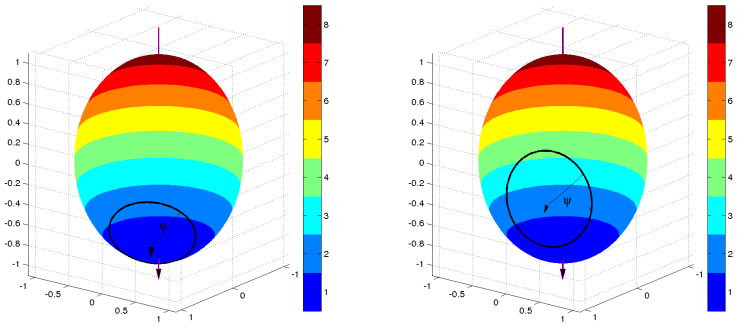

Figure 5: The change in direction-of-motion of electrons scattered with a scattering-angle, ψ, for two different initial picht-angles, and the distribution of new direction-of-motion for the two cases. The coloured unit-sphere illustrates the picth-angle-limits for an eight-stream configuration with uniform steps in μ_l from -1 to 1.

The probability distributions for ψ have been experimentally determined and are compiled into "phase-functions" for elastic and in-elastic collision, which are presented in figure 6. AURORA use phase-functions derived from (Porter et al., n.d.) extended and updated with data from (Linert et al., 2004) for molecular oxygen and (Kanik et al., 2001) for atomic oxygen for elastic and inelastic collisions. For ionizing collisions we make the approximation that the primary high-energy electrons proceed in the forward direction and the secondary electrons produced in the ionization are isotropically distributed. Angular scattering in collisions have an uniform probability distribution in clock-angle around the initial direction of motion as illustrated in figure 7. For a multi-stream electron-transport model it is necessary to calculate the scattering from one stream μ' to another stream μ it is necessary to calculate transition-probabilities from the phase-functions. This is done in steps. The first step is to calculate the fraction of scattering with scattering-angle ψ that falls in stream μ for initial pitch-angles θ. This gives pitch-angle-transition-probability matrices as show in figure 8, where the matrix in each panel shows the probability that an electron with an initial angle, "from-angle", scattering with an angle "scattering-angle" ends up in the labeled stream. These transition-probability matrices can be and are pre-calculated for each pitch-angle configuration. To finaly, calculate the angular re-distribution it is necessary to average the contributions from electrons with all initial pitch-angles within a pitch-angle-stream, for this AURORA uses the assumption that the electron-fluxes are isotropic inside each pitch-angle-stream, that is:

$$I_e(E_i, s, t, \theta) = I_e(E_i, s, t, \mu_l) \sin\theta \Big/ \int_{\theta_l}^{\theta_{l+1}} \sin\theta d\theta.$$

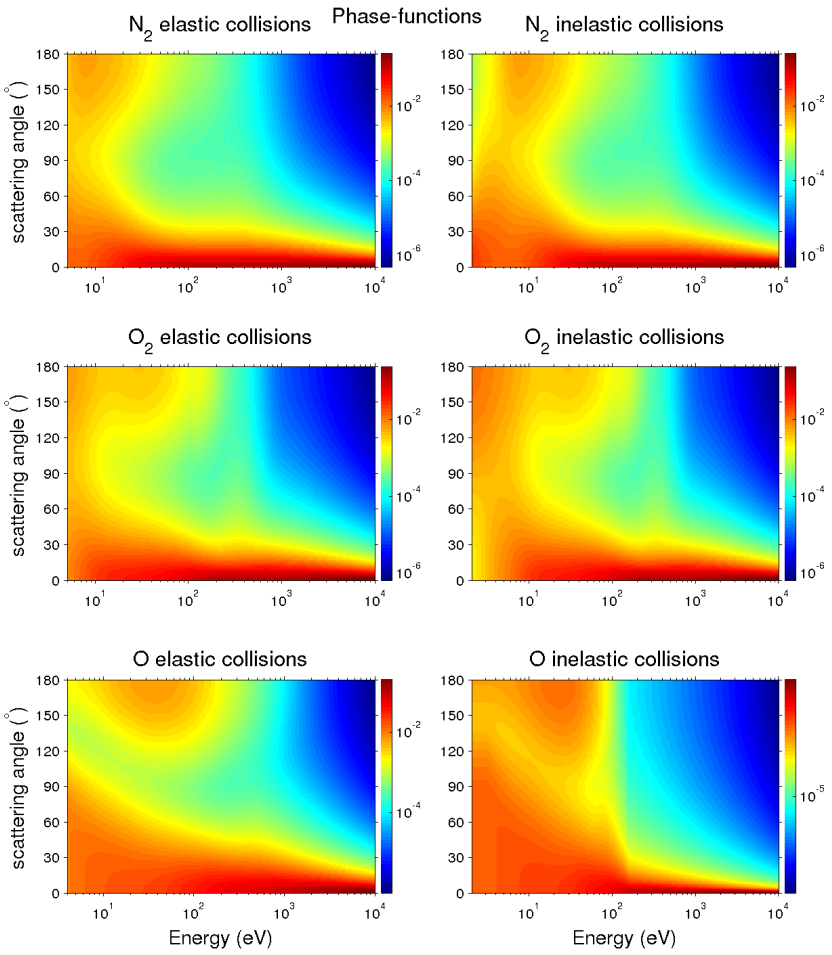

Figure 6: The phase-functions, for elastic (panels in left column) and inelastic (panels in the right column) for molecular nitrogen (top row), molecular oxygen (middle row) and atomic oxygen (bottom row) show the probability distribution for scattering-angles as a function of energy.

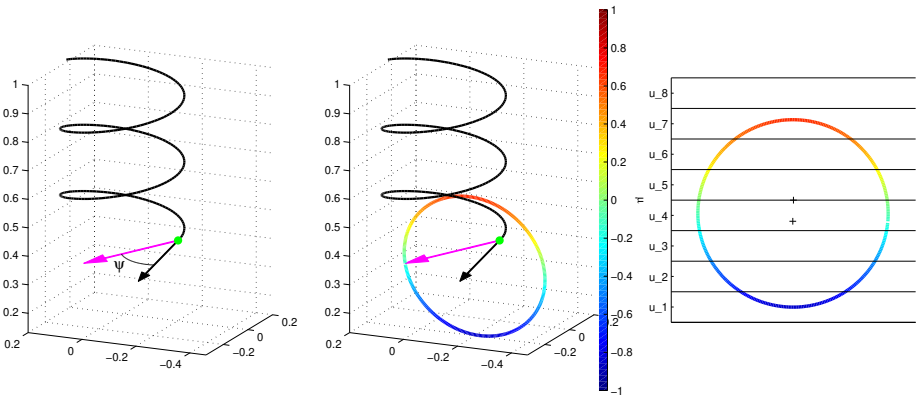

Figure 7: An electron colliding when propagating down along the magnetic field will scatter with some angle ψ, as shown in the left panel. Electrons scattering with angle ψ will have a uniform distribution over the clock-angle around the initial direction-of-motion, as shown in the middle panel, this will give those electrons new pitch-angles, marked with colour. As we use finite-sized pitch-angle-streams the contribution of electrons to each stream will be proportional to the fraction of the cone-of-propagation that falls inside the corresponding pitch-angle limits shown in the right panel.

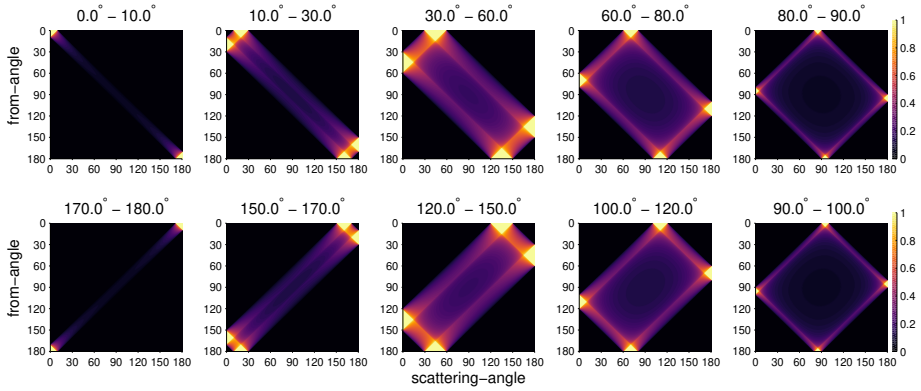

Figure 8: Pitch-angle-transition-probability matrices for the 10-stream pitch-angle-configuration used in the examples. Each panel shows the probability that an electron with an initial pitch-angle, "from-angle" will end up in the corresponding stream after scattering with "scattering-angle".

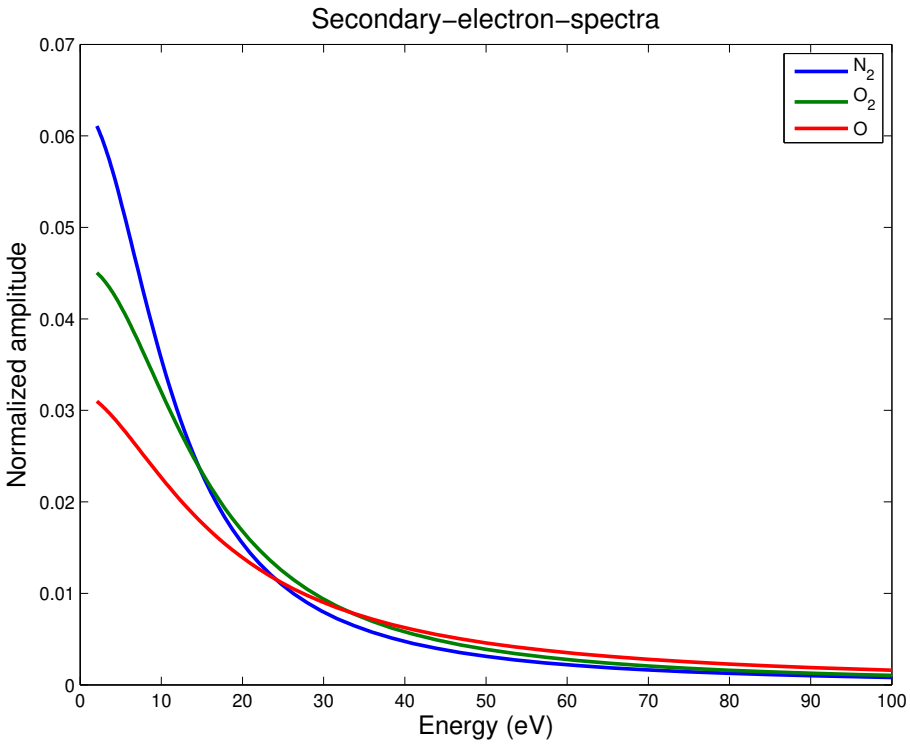

Figure 9: Energy-spectra of secondary electrons produced in electron-collisions with atomic oxygen and molecular oxygen and nitrogen are shown for energies between 0 and 100 eV.

This makes it possible to efficiently calculate the the angular redistribution, modeled with p_k^x in e.g. equation (6) and the A and B_{pq} matrices in equation (7).

For the secondary electrons we use the energy-distributions by Opal, Beaty, and Peterson (1972) for electrons produce in ionization of molecular nitrogen and oxygen. For atomic oxygen we use the analytical fit by (Itikawa & Ichimura, 1990) to the Burnett and Rountree (1979) measurements. The energy distributions are presented in figure 9

A Energy levels of O, O_2, N_2

Table 1: Energy levels of atomic oxygen included in AURORA

State	(eV)
$O^{2+}(^3P)$	48.5
$O^{+}(^2P^0)$	18.6
$O^{+}(^2D^0)$	16.94
$O^{+}(^4S^0)$	13.618
$O(3s'^3D^0)$	12.54
$O(3p^3P)$	10.99
$O(3p^5P)$	10.74
$O(3s^3S^0)$	9.521
$O(3s^5S^0)$	9.14
$O(^1S)$	4.19
$O(^1D)$	1.967
$O(^3P)$	0

Table 2: Energy levels of molecular oxygen included in AURORA

State	$Energy(eV)$
O^{+}+O^{+}	32.51
O^{+}+O	18.9
$O_2^{+}(b^4\Sigma_g^{-})$	18.2
$O_2^{+}(16.9)$	16.9
$O_2^{+}(a^4\pi_u)$	16.1
O+O	15.6
$O_2^{+}(X^2\Pi_g)$	12.072
$O_2(9.97)$	9.97
$O_2(8.4)$	8.4
$O_2(6)$	6.0
$O_2(4.5)$	4.5
$O_2(b^1\Sigma_g^{+})$	1.627
$O_2^{(}a^1\Delta_g)$	0.977
$O_2(vib)$	0.193
$O_2^{2+}(X^3\Sigma_g^{-})$	0.0

Table 3: Energy levels of molecular nitrogen included in AURORA

State	(eV)
$N^+ + N^+$	42
$N + N^+$	24
$N_2^+(B^2\Sigma_u^+)$	18.75
$N_2^+(A^2\Pi_u)$	16.73
$N_2^+(X^2\sigma_g^+)$	15.581
$N + N$	20.6
$N_2(o_3{}^1\Pi_u)$	13.1
$N_2(M1M2)$	13.15
$N_2(G^3\Pi_u)$	12.8
$N_2(F^3\Pi_u)$	12.75
$N_2(D^3\Sigma_u^+)$	12.85
$N_2(C'^3\Pi_u)$	12.08
$N_2(c_4'{}^1\Sigma_u^+)$	12.94
$N_2(b'^1\Sigma_u^+)$	12.85
$N_2(C^3\Pi_u)$	11.032
$N_2(a^1\Pi_g)$	8.5489
$N_2(a''^1\Sigma_g^+)$	12.255
$N_2(E^3\Sigma_g^+)$	11.875
$N_2(w^1\Delta_u)$	8.8895
$N_2(a'^1\Sigma_u^-)$	8.3987
$N_2(B'^3\Sigma_u^-)$	8.1647
$N_2(w^3\Delta_u)$	7.3622
$N_2(B^3\Pi_g)$	7.3532
$N_2(A^3\Sigma_u^+)$	6.1688
$N_2(vib: 0 \to 7)$	1.9475
$N_2(vib: 0 \to 6)$	1.6801
$N_2(vib: 0 \to 5)$	1.4088
$N_2(vib: 0 \to 4)$	1.1342
$N_2(vib: 0 \to 3)$	0.8559
$N_2(vib: 0 \to 2)$	0.5742
$N_2(vib: 0 \to 1)$	0.2888
$N_2(rot: 0 \to 8)$	0.017765
$N_2(rot: 0 \to 6)$	0.010362
$N_2(rot: 0 \to 4)$	0.0049339
$N_2(rot: 0 \to 2)$	0.0014801
$N_2(X^1\Sigma_g^+)$	0

References

Burnett, T., & Rountree, S. P. (1979). Differential and total cross sections for electron-impact ionization of atomic oxygen. *Physical Review A*, *20*(4), 1468.

Gronoff, G., Simon Wedlund, C., Mertens, C. J., & Lillis, R. J. (2012). Computing uncertainties in ionosphere-airglow models: I. electron flux and species production uncertainties for mars. *J. Geophys. Res.*, *117*, A04306. doi: 10.1029/2011JA016930

Guio, P. (1998). *Studies of ionospheric parameters by means of electron plasma lines observed by eiscat* (Unpublished doctoral dissertation). University of Tromsø, Université Joseph-Fourier-Grenoble I.

Hedin, A. (1991, February). Extension of the MSIS thermospheric model into the middle and lower atmosphere. *J. Geophys. Res.*, *96*(A2), 1159-1172.

Itikawa, Y., Hayashi, M., Ichimura, A., Onda, K., Sakimoto, K., Takayanagi, K., ... Takayanagi, T. (1986). Cross sections for collisions of electrons and photons with nitrogen molecules. *J. Phys. Chem. Ref. Data*, *15*(3), 985-1010.

Itikawa, Y., & Ichimura, A. (1990). Cross sections for collisions of electrons and photons with atomic oxygen. *J. Phys. Chem. Ref. Data*, *19*(3), 637-651.

Itikawa, Y., Ichimura, A., Onda, K., Sakimoto, K., Takayanagi, K., Hatano, Y., ... Tsurubuchi, S. (1989, January). Cross Sections for Collisions of Electrons and Photons with Oxygen Molecules. *Journal of Physical and Chemical Reference Data*, *18*, 23-42.

Kanik, I., Johnson, P. V., Das, M. B., Khakoo, M. A., & Tayal, S. S. (2001, July). Electron-impact studies of atomic oxygen: I. Differential and integral cross sections; experiment and theory. *Journal of Physics B Atomic Molecular Physics*, *34*, 2647-2665.

Linert, I., King, G. C., & Zubek, M. (2004, December). Measurements of differential cross sections for elastic electron scattering in the backward direction by molecular oxygen. *Journal of Physics B Atomic Molecular Physics*, *37*, 4681-4691. doi: 10.1088/0953-4075/37/23/009

Opal, C., Beaty, E., & Peterson, W. (1972). Tables of secondary-electron-production cross sections. *Atomic Data and Nuclear Data Tables*, *4*, 209–253.

Peticolas, L., & Lummerzheim, D. (2000, June). Time-dependent transport of field-aligned bursts of electrons in flickering aurora. *J. Geophys. Res.*, *105*(A6), 12895-12906.

Picone, J. M., Hedin, A. E., Drob, D. P., & A.C. Aikin, A. C. (2002). Nrlmsise-00 empirical model of the atmosphere: Statistical comparisons and scientific issues. *J. Geophys. Res.*, *107*(A12), 1468. doi: 10.1029/2002JA009430

Porter, H. S., Varosi, F., & Mayr, H. G. (n.d.). Iterative solution of the multistream electron transport equation: 1. comparison with laboratory beam injection experiments. *Journal of Geophysical Research: Space Physics*, *92*(A6), 5933-5959. Retrieved from `https://agupubs`

.onlinelibrary.wiley.com/doi/abs/10.1029/JA092iA06p05933 doi: 10.1029/JA092iA06p05933

Schunk, R., & Nagy, A. (2009). *Ionospheres: physics, plasma physics, and chemistry*. Cambridge university press.

Swartz, W. E., Nisbet, J. S., & Green, A. E. S. (1971, Dec). Analytic expression for the energy-transfer rate from photoelectrons to thermal electrons. *J. Geophys. Res.*, *76*(34), 8475-8480.